A QUICK OVERVIEW OF A NEW SCINTILLATION DATABASE

Ana Pinho, Susana Mota, Armando Rocha
Departamento de Eletrónica, Telecomunicações e Informática/Instituto de Telecomunicações, Universidade de Aveiro, Campus Universitário Santiago 3810 193, Portugal

Abstract *– This paper explores a new Ka and Q-band dry scintillation database and ancillary meteorological data collected at Aveiro, Portugal in two converging Earth-satellite propagation paths. The measurement equipment, the parameters of both links and the processing procedure of the database are described first. The dependencies of the hourly averaged scintillation standard deviation with respect to several meteorological parameters, measured at the ground level, and with respect to the wet refractive index are analyzed. The diurnal variation of the hourly averaged scintillation standard deviation, on a monthly and yearly basis, is explored. The yearly amplitude distributions, fades and enhancements, are presented and compared against some available models. The scatter plot of the concurrent hourly averaged scintillation standard deviation is analyzed and a frequency scaling factor is tentatively derived.*

Keywords – Diurnal variability, modeling, scintillation

1. INTRODUCTION

A microwave signal crossing the atmosphere is subjected to several impairments such as attenuation, depolarization and scintillation. The scintillation is caused by the scattering of atmospheric refractive index irregularities in turbulent layers that evolve over time and drift through the propagation path carried by the wind. The phase and amplitude distorted wave front is integrated by the receiving antenna aperture giving rise to the observed signal amplitude fluctuations (phase fluctuations are more difficult to measure) around a mean value computed typically in 1 minute to 5 minutes.

The modeling of scintillation is important because it can disturb the fade mitigation systems and the scintillation fades can impact the availability of terminals with very small fade margins.

Scintillation long term data at Q-band and databases collected with concurrent satellite links are yet relatively scarce in the literature.

2. EXPERIMENTAL SCENARIO

Two propagation experiments have been active at our site: one using the Ka-Sat satellite Ka-band beacon at 19.68 GHz and the other with the Alphasat satellite Q-band beacon at 39.402 GHz. The receivers use FFT techniques for signal detection whose samples are stored, in both cases, at a rate of 8S/s. More information can be found in [1]. The receivers are fully independent; they do not share any hardware.

The general characteristics of the links are given in the following table: where the CNR_0 (dB-Hz) is the carrier to noise spectral density ratio in clear sky.

Table 1 – Ka and Q-band receiver characteristics

Parameter	Ka-Band	Q-band
Antenna diameter (m)	1.50	0.62
Elevation(º)	39.63	31.9
Azimuth (º)	153.95	134.6
CNR_0 (dB-Hz)	53.0	57.7
Polarization quasi-V (º): tilt angle	19.5	12.3
Sampling rate (S/s)	8	8

The site coordinates are 40^0 37′ N and 8^0 39’ W being the Q-band receiver about 3 m below the Ka-band receiver (in an office below the roof). The angular aperture between the two links is about 17^0. Recently the K-band receiver front-end was refurbished and the CNR_0 has been improved by about 4 dB. A small meteorological station is also co-sited and measures temperature, relative humidity, rain rate, wind speed and atmospheric pressure at the ground level.

Q-band data are logged by a *MATLAB* application into a set of files and the Ka-band beacon and meteorological data are logged by a *Labview* application into another set of files. The beacon data copolar amplitude time series is stored at a sampling rate of 8 S/s.

3. DATA ANALYSIS

The raw experimental data is loaded together and preprocessed by a dedicated tool to perform the preprocessing [2]. This step aims to check the quality of the data and to derive the attenuation by using the measured copolar levels and the estimated copolar levels that would be observed in the absence of attenuation. All preprocessed time series are stored in a single daily file.

For the scintillation analysis, first, the preprocessed data files are loaded and the scintillation time series is obtained by using a high pass filter, based on raised cosine with a 0.025 Hz cut-off frequency. Then, the wet refractivity, N_{wet}, is calculated using the temperature, T(ºC), relative humidity, H(%), and pressure, P(hPa), all integrated with a 10 minutes integration time, according to [3]:

$$N_{wet} = 72\frac{e}{T+273} + 3.75x10^5\frac{e}{(T+273)^2} \qquad (1)$$

The water vapor pressure, e(hPa), is related with H by

$$e = \frac{e_s H}{100}\,(\text{hPa}) \qquad (2)$$

The water vapor saturation pressure, e_s, can be calculated from the temperature and the pressure but the equations also found at [3], are omitted here for brevity.

The scintillation variance is calculated in one-minute non-overlapping time windows. Finally, the scintillation time series and the processed meteorological data are stored in a new file. Statistical data on scintillation parameters is derived by dedicated tools that have been developed in *MATLAB*.

It must be pointed out that, due to the finite CNR_0, the Gaussian noise introduces a bias on the scintillation variance, given by [4]:

$$\sigma_n^2 = 75.44x10^{-\frac{CNR-10log_{10}(f_S)}{10}}\,(\text{dB}^2) \qquad (3)$$

where $f_s = 8$ Hz is the sampling bandwidth. The calculations, using the values in Table 1, gives respectively, 1.0E-3 and 3.0E-3 dB² for the Q and Ka bands.

The measured variance, σ_m^2, is related to the atmospheric induced variance, σ_{atm}^2, by the equation:

$$\sigma_m^2 = \sigma_{atm}^2 + \sigma_n^2\,(\text{dB}^2) \qquad (4)$$

The variance (or standard deviation) presented throughout the paper, is σ_m^2. The accurate removal of the noise contribution must yet be carefully addressed due to CNR variations along the time; however, its contribution to the variance is small.

4. RESULTS AND ANALYSIS

The scintillation is usually characterized by the distribution of the amplitude, χ (dB), or by the standard deviation, σ_χ, computed in 1-minute time windows. This last one is often calculated only for dry periods, therefore, the periods with attenuation larger than 0.5 dB at Ka-band and 1 dB at Q-band were excluded from the statistical calculations. The annual and monthly statistics here presented correspond to a full year, from June 2017 to May 2018.

4.1 Meteorological dependencies

The joint distributions of the hourly averaged scintillation standard deviation and meteorological parameters were calculated.

Fig. 1 presents the Q-band scintillation standard deviation versus the atmospheric pressure. The higher the pressure the lower the scintillation variance. High pressure means usually clear sky, dry and stable weather: conditions that are not prone to atmospheric instability. As we can see the higher the scintillation standard deviation is, the more sensitive to the pressure. The scintillation variance is higher than the minimum expected value due to measurement noise (see Section 3), therefore, a residual scintillation is always present. The hourly correlation between the two-time series is already not negligible. A similar plot is obtained for the Ka-band.

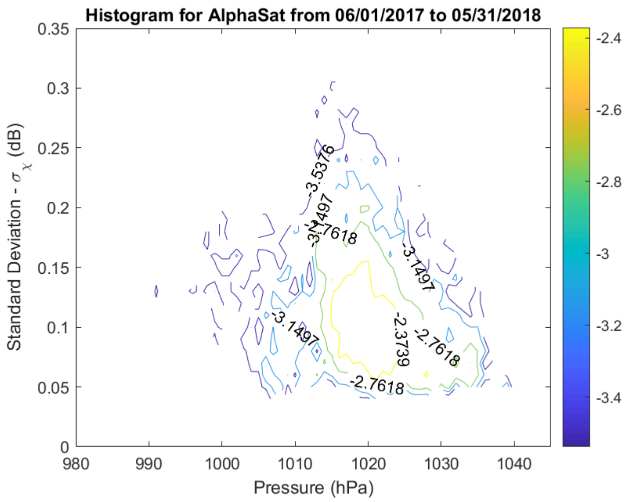

Fig. 1 – Joint histogram (in log. units) of the scintillation standard deviation at Q-band vs atmospheric pressure; the contours are log spaced

Fig. 2 shows the scintillation standard deviation at Ka-band versus N_{wet}. As we can see, there is also a clear correlation with N_{wet}; the higher the wet refractivity the higher the scintillation standard deviation. The N_{wet} parameter, averaged on a long term basis, has been used to model the distribution of the scintillation standard deviation[5]–[7].

Fig. 3 depicts the scintillation standard deviation at the Q-band versus temperature. There is a clear trend that shows the effect of the temperature; the higher the temperature the higher the scintillation standard deviation. That is, higher temperatures are associated with increased atmospheric instability. Exactly the same trend is observed at Ka-band (not depicted).

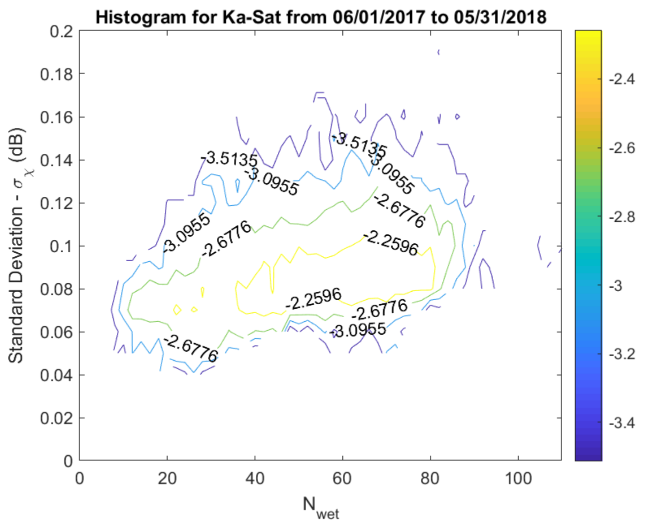

Fig. 2 – Joint histogram (in log.units) of the standard deviation at Ka-band vs Nwet; the contours are log spaced

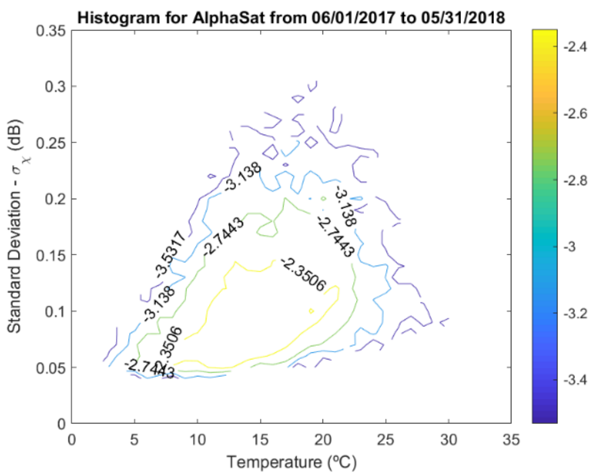

Fig. 3 – Joint histogram (in log units) of the standard deviation at Q-band vs temperature; the contours are log spaced

The correlation of the standard deviation with the several meteorological related variables is summarized in Table 2.

Table 2 – Correlation between scintillation standard deviation and meteorological parameters

Meteorological parameter	Correlation Ka-band	Correlation Q-band
Pressure (mB)	−0.31	−0.29
Nwet	0.33	0.34
Temperature (ºC)	0.34	0.36
Water vapor (g/m³)	0.33	0.35
Relative humidity	0.14	0.12

The most uncorrelated variable is the relative humidity. The variables N_{wet}, temperature and water vapor content have similar correlations being the corresponding correlations at Q-band slightly higher. The models usually use meteorological parameters averaged on longer periods as input data, however, a noticeable correlation is observed with hourly data. The Ortgies-T [8] and Marzano [9] models seem to deserve attention as the correlation of the standard deviation with temperature is similar to that of the usually used N_{wet} as a modeling parameter.

4.2 Diurnal variation

The diurnal variation of the standard deviation (the time is given in UTC) has been calculated on a monthly and yearly basis. The trend is the same along all months with somewhat more striking diurnal variations during the months with average higher temperatures.

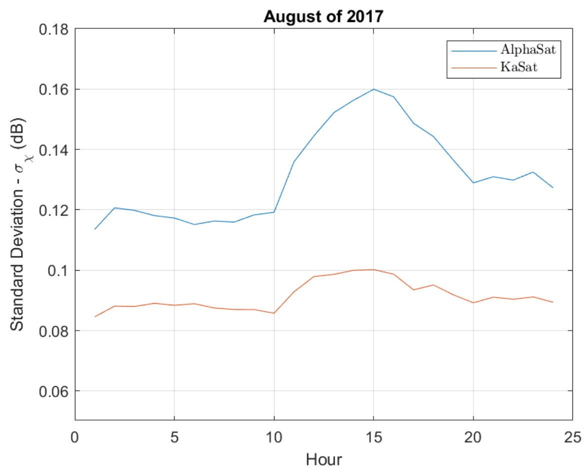

Fig. 4 – Hourly average values of the scintillation standard deviation at the Q and Ka bands in August 2017

The most scintillating periods of the day are from 10 am to 8 pm as can be observed in Fig. 4; this latter hour occurs a little bit earlier during winter.

Often, higher scintillation periods, however not as intense as those of the afternoon, also occur close to midnight, usually after, as can be observed in Fig. 5. The lowest scintillation periods occur from 5 am to 9 am and 10 pm to 11 pm. Some turbulent processes must be occurring in the atmosphere between the more quite end of the day and the early morning. The day variations are very similar at both frequencies as can be easily observed.

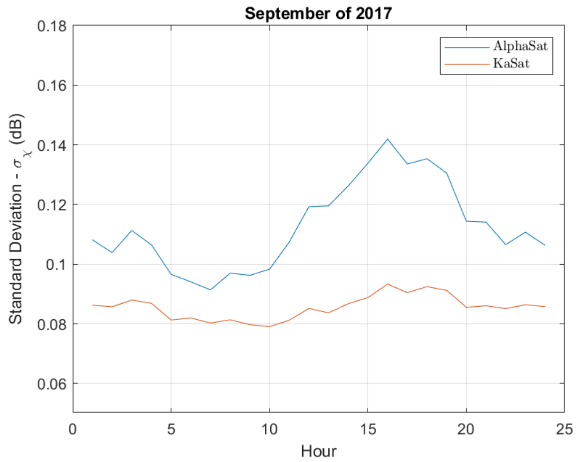

Fig. 5 – Hourly average values of the scintillation standard deviation at the Q and Ka band: September 2017

Lowest scintillation periods occur during the coldest months with clear sky, foggy weather, very dry periods (even windy ones) and, in addition, with very weak and long lasting rain, mainly drizzle. The worst and most sustained scintillation periods occur during uniform cloud cover and hot weather, not necessarily leading to rain. Burst scintillation periods are observed during showery weather with dense and sparse clouds; often a rain shower is preceded by an increased scintillation period that is probably due to turbulence in developing rain cells, caused by air masses down/updrafts and shear winds.

4.3 Distribution of fades and enhancements

The monthly distribution of the scintillation amplitude enhancements, χ^+ (dB), and fade depth, χ^-, for a full year are depicted, respectively, in Fig. 6 and Fig. 7 for the Q-band.

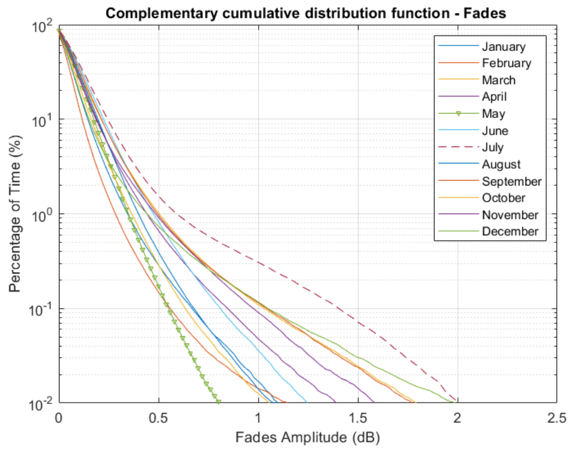

Fig. 6 – Monthly cumulative distributions of the fades for the Q-band (one year: June 2017 to May 2018)

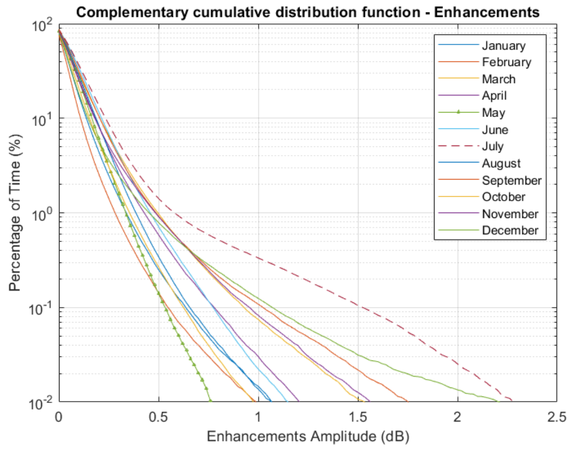

Fig. 7 – Monthly cumulative distributions of the enhancements for the Q-band (one year: June 2017 to May 2018)

As discussed in [4] for the same probability the fades are, in general, deeper than the enhancements. However, in spite of being true along an average year, the difference is very small and it is not verified for all the months.

There is a significant variability of the cumulative distributions from month to month but there is no clear distinction between late spring, summer and early fall from the other periods. Higher temperatures but clear sky and higher pressures are balanced by lower temperature but often cloudier conditions during the other periods.

4.4 Concurrent standard deviation at the two bands

As described above the two converging links have an angular difference of about 17º and the distance between the points where the links cross a plane at 1000 m altitude is several hundreds of meters. Nevertheless, a very high correlation between the scintillation variance at the two frequencies has been always observed. This means that the spatial stationarity of the turbulence is of the same order of the distance between the points where the links cross the turbulence.

Fig. 8 depicts the high correlation mentioned above, with the peculiarity that the Ka-band receiver has been upgraded during this month; for the last 10 days of the month a higher CNR_0 was already available. It is notorious that the presence of two data sets being the lower set collected already with the better CNR_0 estimated to be about 6.5 dB wrt to the actual performance of the receiver (the receiver NF had a fast CNR degradation during the last two months of operation).

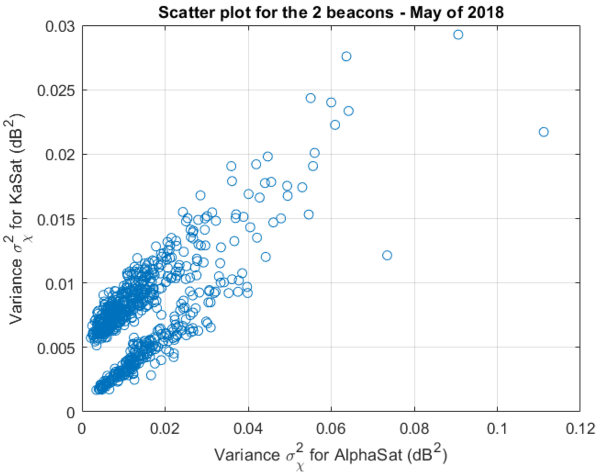

Fig. 8 – May 2018 scatter plot of the hourly averaged scintillation variance at the two frequencies; CNR improvement is observed

The annual scatter plot results presented in Fig. 9 show the high correlation between the two variances that were, nevertheless, expected from the diurnal variation discussion in section 11. The obtained annual correlation was 0.772 and is quite similar throughout all the months.

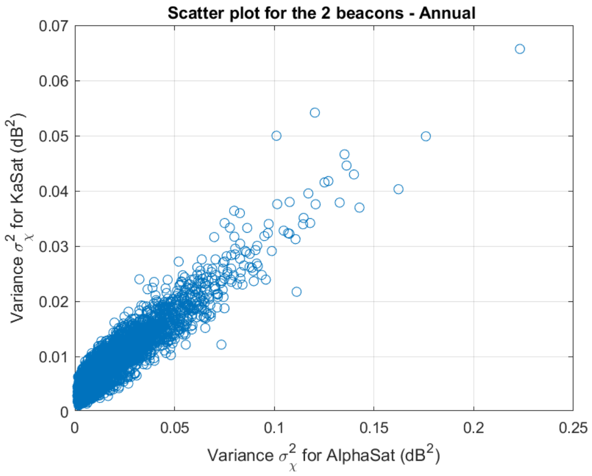

Fig. 9 – Year scatter plot of the hourly averaged scintillation variance at the two frequencies

A frequency scaling factor for the variance was estimated, for example for the April data depicted in Fig. 10, by performing a linear fitting to the variances scatter plot. A value of 0.288 was obtained for the slope that is very close to the variance scaling factor obtained by using the frequencies, elevation angles and antenna reduction factors that can be found in several models.

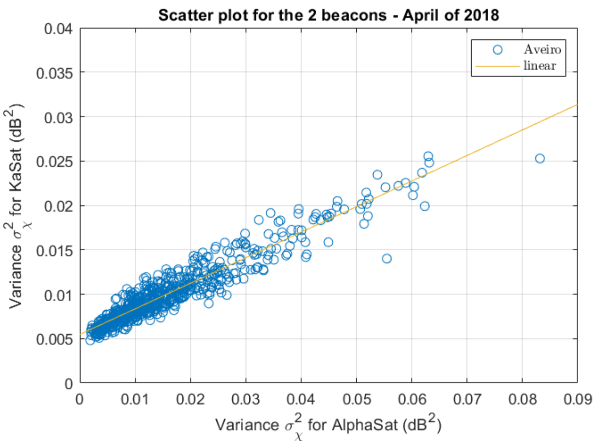

Fig. 10 – A month scatter plot of the variance at the two bands and a linear fitting to the data

5. SCINTILLATION MODELS

A few essays of some available scintillation models have been performed, such as, the scintillation fades and enhancements using the Otung [7], ITU [10] (only for fades), van de Kamp [11] and the Karasawa [5] models. Fig. 11 and Fig. 12 were obtained for the Ka-band using the yearly average measured N_{wet} =51.5, the antenna variance averaging factors of about 0.86 and 0.95 (respectively for the Ka and Q-band) computed for a turbulent layer height of 1 km (ITU and Otung models) and 2 km (for the Karasawa model) and, finally, assuming the antennas efficiency of 60%. The long term average water content W_{hc} of heavy clouds, used in the van de Kamp model, was roughly estimated as 1 kg/m^2 from [12].

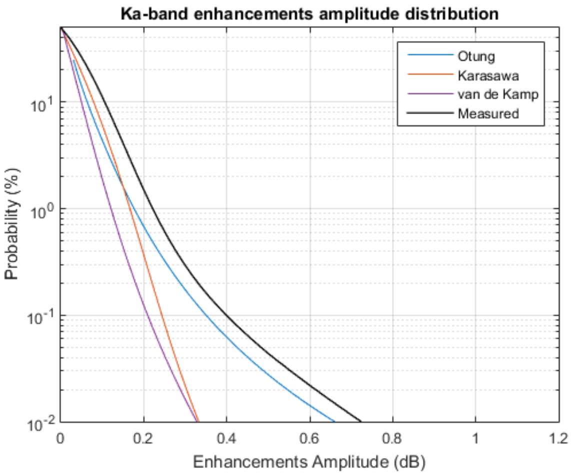

Fig. 11 – Cumulative distribution of the enhancements at Ka-band and the predictions of the models for one year

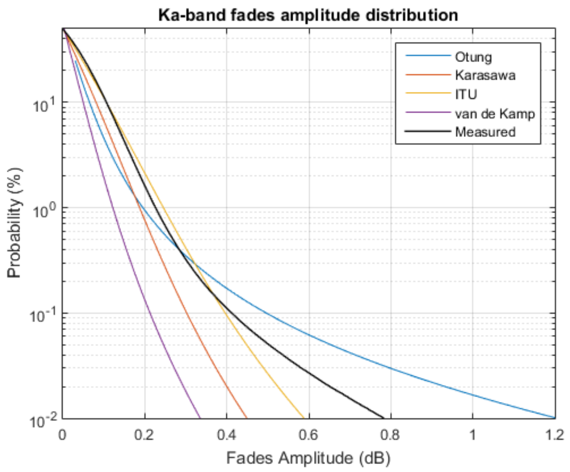

Fig. 12 – Cumulative distribution of the fades at Ka-band and the predictions of the models for one year

The Otung model seems to give the better predictions for the enhancements while the van de Kamp and Karasawa models under-predicts both the fades and enhancements. The ITU model performs reasonably well with the fades. The performance of the available models will be systematically evaluated in future work.

6. CONCLUSION

A scintillation database has been collected at Aveiro, Portugal at Ka and Q-band in convergent links. In spite of an already existing database at Ka-band, the new one now comprises the Q-band. The experimental conditions were described in detail to understand the potentials and limitations of the database.

The correlation of the hourly averaged scintillation standard deviation and local meteorological data has been analyzed. A positive correlation was found with ambient temperature and the water vapor density and a negative one with the atmospheric pressure.

The diurnal variation is more observable during the summer months and the scintillation is more intense from 10 am to 8 am. The monthly fade and enhancements distributions show a significant variability. There is a high correlation between the hourly scintillation variance at the two frequencies in spite of the angular separation of the two links. The variance frequency scaling seems to be well described by the theory. The best fade and enhancements model to describe the experimental data seems to be the Otung one.

ACKNOWLEDGEMENT

This work was developed in the framework of the European Space Agency (ESA) funded project Large Sale Assessment of Ka/Q Band Atmospheric Channel Using the Alphasat TDP5 Propagation Beacons, ESA ITT AO/1-7963/14/NL/LvH.

The authors are grateful to ESA and ESA Technical Officer, Dr. Antonio Martelluci, for funding the refurbishment of the Ka-band terminal front-end which extends significantly the receiver dynamic range.

REFERENCES

[1] A. Rocha, T. Pereira, S. Mota, and F. Jorge, “Alphasat experiment at Aveiro,” in 2016 10th European Conference on Antennas and Propagation (EuCAP), 2016, pp. 1–5.

[2] J. Flávio, A. Rocha, S. Mota, and F. Jorge, “Alphasat Experiment at Aveiro : Data Processing Approach and Experimental Results,” in European Conference on Antennas and Propagation, 2017, pp. 2376-2380.

[3] Rec. ITU-R P.453-13, “The radio refractive index : its formula and refractivity data P Series Radiowave propagation,” vol. 13, 2017.

[4] M. M. J. L. van de Kamp, “Climatic Radiowave Propagation Models for the design of Satellite Communication Systems,” Eindhoven University of Technology, 1999.

[5] Y. Karasawa, M. Yamada, and J. E. Allnutt, “A new prediction method for tropospheric scintillation on Earth-space paths,” IEEE Trans. Antennas Propag., vol. 36, no. 11, pp. 1608–1614, 1988.

[6] M. M. J. L. Van De Kamp, C. Riva, J. K. Tervonen, and E. T. Salonen, “Frequency dependence of amplitude scintillation,” IEEE Trans. Antennas Propag., vol. 47, no. 1, pp. 77–85, 1999.

[7] I. E. Otung, “Prediction of tropospheric amplitude scintillation on a satellite link,” IEEE Transactions on Antennas and Propagation, vol. 44, no. 12. pp. 1600–1608, 1996.

[8] G. Ortgies, “Prediction of Slant-Path Amplitude Scintillations from Meteorological Parameters,” in International Symposium on Radio Propagation(ISRP’93), 1993.

[9] F. S. Marzano, C. Riva, A. Banich, and F. Clivio, “Assessment of model-based scintillation variance prediction on long-term basis using Italsat satellite measurements,” Int. J. Satell. Commun., vol. 17, no. 1, pp. 17–36, Jan. 1999.

[10] Rec ITU-R P.618-13, “Propagation data and prediction methods required for the design of Earth-space telecommunication systems,” 2009.

[11] M. M. J. L. van de Kamp, “Asymmetric signal level distribution due to tropospheric scintillation,” Electron. Lett., vol. 34, no. 11, pp. 1145, 1998.

[12] M. M. J. L. van de Kamp, J. K. Tervonen, E. T. Salonen, and J. P. V. Poirares Baptista, “Improved models for long-term prediction of tropospheric scintillation on slant paths,” IEEE Trans. Antennas Propag., vol. 47, no. 2, pp. 249–260, 1999.